

Short Communication

## Corrosion Resistance of Super-Hydrophobic Coating on AZ31B Mg Alloy

Zhengwei Song<sup>1</sup>, Zhihui Xie<sup>2,\*</sup>, Lifeng Ding<sup>1</sup>, Yike Zhang<sup>1</sup>

<sup>1</sup> Department of Chemistry and Chemical Engineering, Taiyuan Institute of Technology, Taiyuan 030024, Shanxi, China

<sup>2</sup> Chemical Synthesis and Pollution Control Key Laboratory of Sichuan Province, China West Normal University, Nanchong 637002, Sichuan, China

\*E-mail: [zhxie@cwnu.edu.cn](mailto:zhxie@cwnu.edu.cn)

Received: 31 March 2018 / Accepted: 8 May 2018 / Published: 5 June 2018

A super-hydrophobic coating was prepared on AZ31B Mg alloy in this paper. Electroless Ni-P coating as the inner layer was deposited on the AZ31 substrate via an electroless plating process, and Cu was electroplated as the intermediate layer. Then, the electroplating Ni method was employed to form the micro/nano structure, and the super-hydrophobic coating was prepared after the composite coating modified by stearic acid. The modified coating exhibited super-hydrophobic properties with a static water contact angle of 155°. Potentiodynamic polarization and electrochemical impedance spectroscopy (EIS) tests were conducted in 3.5 wt.% NaCl solution at room temperature. The test results indicated that the corrosion resistance of AZ31 was improved significantly by this super-hydrophobic coating. The super-hydrophobic samples had much more corrosion resistance in comparison with freshly prepared samples.

**Keywords:** Corrosion resistance; Super-hydrophobic; Mg alloy

### 1. INTRODUCTION

Mg alloy, as the lightest alloy, has attracted industrial interest due to its high castability, low density, bio-compatibility, and so on [1]. Magnesium alloys are intensively applied in the 3C, automobile and clinical medicine fields. However, the high chemical reactivity of magnesium alloys leads to poor corrosion resistance that limits its more widespread applications. Therefore, how to enhance the corrosion resistance of magnesium and its alloys has been widely studied[2-6] .

Various surface treatment methods have been studied to enhance the corrosion resistance of magnesium alloys[7-10]. Super-hydrophobic surfaces, with a water contact angle (CA) larger than 150°, have attracted particular interest of researchers due to the widespread potential applications in

the fields of coatings, textiles, construction, and so on. Using super-hydrophobic surfaces as a new method to improve the corrosion performance of metals has been reported in recent years[11-16]. Super-hydrophobic coatings have been successfully prepared on the surfaces of various engineering materials, such as Fe, Al and Cu. This coating acts as a barrier layer that can reduce the portion of real contact between the corrosive electrolyte and the metal surface[17]; hence, the corrosion resistance of pre-treated substrate is better than before. As we know, the corrosion of Mg or Mg alloys usually occurs in the presence of water, and it is significant to prepare an anticorrosion super-hydrophobic surface on the Mg alloy surface for wide application of magnesium alloys.

To prepare super-hydrophobic coatings on metal surfaces, the following two conditions should be met simultaneously[18]: first, a rough surface with hierarchical rough structures is required; second, the material on the surface layer has to have low surface energy. Hence, super-hydrophobic surfaces are often fabricated via two processes[19]: (1) creation of micro/nanometre-scale binary rough structures on the surface; and (2) modification of an appropriate rough surface with low surface energy materials.

In this paper, a simple method was designed for fabricating a super-hydrophobic coating on AZ31B Mg alloy. The fabrication process of the super-hydrophobic surface mainly contains four steps: electroless Ni-P coating, electrodeposition of Cu, electrodeposition of Ni, and modification. The uniform electroless Ni-P coating as an inner layer can protect the substrate, and electrodeposition of Cu provides a uniform distribution of the electric field for the Ni electrodeposition process. Then, the process of Ni electrodeposition creates a micro/nanometre-scale binary rough structure surface. The samples were then modified by immersing in 1 wt.% ethanol solution of stearic acid to reduce the surface energy. The corrosion behaviour of this coating was also explored in this paper.

## 2. EXPERIMENT

### 2.1 Materials

Commercial AZ31B (wt.%: 3% Al, 1% Zn, 0.2% Mn, Fe < 0.005%, balanced Mg) was purchased from Hong Di Metal Materials Co., Ltd (Dongguan, China). All chemical reagents were obtained from Sinopharm Chemical Reagent Co., Ltd. and were used as received.

### 2.2 Specimen preparation

AZ31 Mg alloy with dimensions of 20×30×1.5 mm was ground with SiC paper with different grit sizes (240, 600, 1200#) successively and then washed with distilled water and acetone step by step.

### 2.3 Coating preparation

The process flow and the main parameters for the pretreatment and electroless Ni-P coating were introduced in our previous studies[20-22], and the conditions for electroplating Cu and

electroplating Ni are listed in Table 1. The samples were cleaned thoroughly with deionized water as quickly as possible between any two steps of the treatments.

**Table 1.** The bath composition and operation conditions of electroplating Cu and Ni

Process	Composition	Contents	Conditions
Electroplating Cu	$\text{Cu}_2\text{P}_2\text{O}_7$	$60 \text{ g}\cdot\text{dm}^{-3}$	$0.8\sim 1 \text{ A}\cdot\text{dm}^{-2}$
	$\text{K}_4\text{P}_2\text{O}_7\cdot 3\text{H}_2\text{O}$	$290 \text{ g}\cdot\text{dm}^{-3}$	15 min
	$(\text{NH}_4)_3\text{C}_6\text{H}_5\text{O}_7$	$25 \text{ g}\cdot\text{dm}^{-3}$	pH=9±0.5 45±2 °C
Electroplating Ni	$\text{NiCl}\cdot 6\text{H}_2\text{O}$	$237 \text{ g}\cdot\text{dm}^{-3}$	$2 \text{ A}\cdot\text{dm}^{-2}$
	$\text{H}_3\text{BO}_3$	$31 \text{ g}\cdot\text{dm}^{-3}$	1-15 min
	Ethylene diamine hydrochloride	$140 \text{ g}\cdot\text{dm}^{-3}$	pH=4.0±0.5 60±2 °C

## 2.4 Surface characterization

The morphology of the coatings was characterized by Field Emission Scanning Electron Microscopy (FE-SEM) complemented by energy dispersive spectroscopy.

X-ray diffraction (XRD) with a Cu target was employed to characterize the crystal texture of different coatings.

## 2.5 Electrochemical tests

The electrochemical workstation (PMC 2000, Princeton, USA) was used to research the electrochemical corrosion behaviour of the samples. All electrochemical measurements were measured by a three-electrode system at room temperature. The pre-treated samples as the working electrode were embedded in epoxy resin, and the surface with a  $10\times 10 \text{ mm}^2$  area as the effective working side was exposed. The Pt electrode and saturated calomel electrode were used as the reference and counter electrodes. In general, 3.5 wt.% NaCl aqueous solution as the corrosive medium was used in all electrochemical corrosion measurements.

Electrochemical impedance spectroscopy (EIS) and the electrochemical polarization curve were tested to evaluate the extent of corrosion in 3.5 wt.% NaCl solution. EIS was tested at an open circuit potential of 5 mV and AC amplitude in the frequency region from 100,000 to 0.01 Hz. The electrochemical polarization curve was obtained at room temperature with a potential scanning rate of  $1 \text{ mV}\cdot\text{s}^{-1}$  from cathodic to anodic in the potential range from the open circuit potential to  $\pm 400 \text{ mV}$ . The tests were repeated three or more times to ascertain the creditability of the test results.

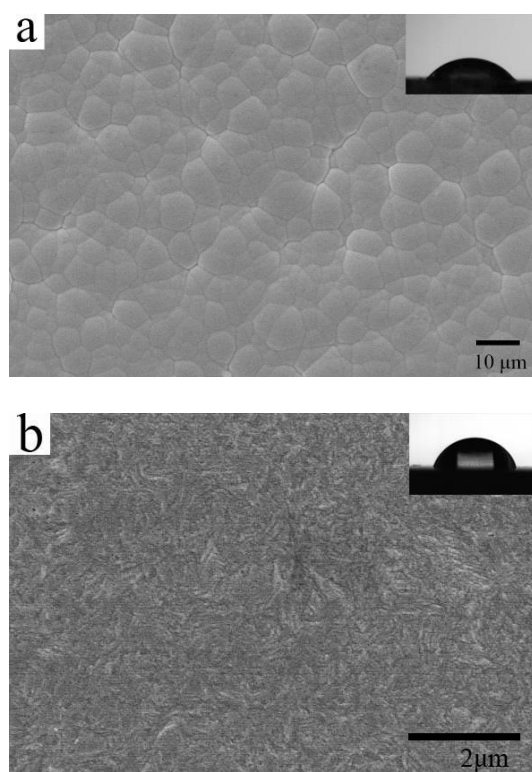
## 2.6 Contact angle measurement

A contact angle meter was used to measure the water contact angles (CAs) at room temperature. Five or more different points were measured to calculate the average value reported as the CA value.

## 3. RESULTS AND DISCUSSION

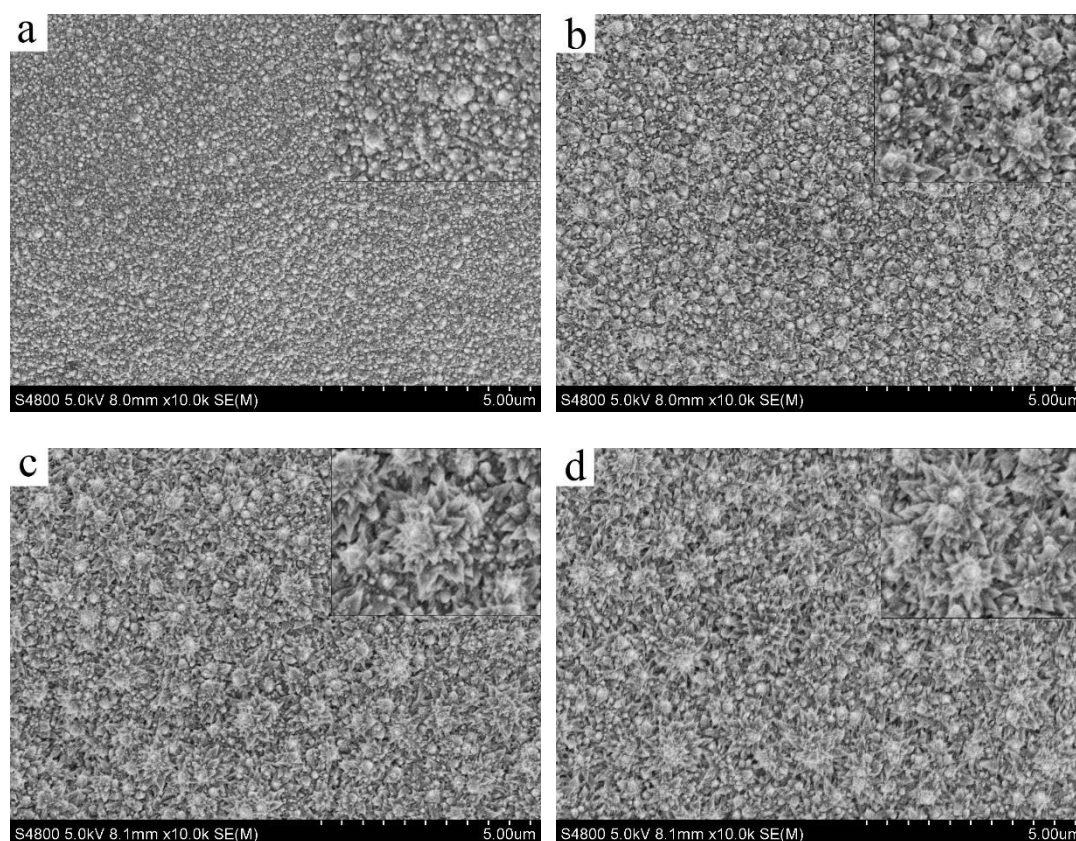
### 3.1 The preparation of the nanometre-scale Ni coating

Figure 1 shows the morphology of the Ni-P and Cu coatings on AZ31B. The distribution of the nodular structure on the Ni-P surface is uniform as shown in Figure 1, and the size of the nodular structure is in the range of 5-10  $\mu\text{m}$ . No cracks and pores were seen on both the nodular structural surface and on the border of the two nodular structures. The surface became smoother through electroplating Cu for 15 min (as shown in Figure 1b), and no visible nodular structure can be detected. The uniform coating can provide a uniform electric field distribution for electroplating Ni. After 20 cycles of the thermal shock experiment according to ASTM B733-04, no blistering, crinkling, or breakage was observed at 4 times magnification[23]. The result shows that the adhesion of the Ni-P/Cu coating is excellent. In the next process of electroplating, the compact and uniform coating of Ni-P/Cu could protect the substrate from corrosion. The CAs of Ni-P and Cu are about  $52^\circ$  and  $70^\circ$ , which indicated that the Ni-P and Cu coatings are hydrophilic coatings.



**Figure 1.** The morphology of electroless Ni-P and electroplated Cu coatings: a: Ni-P; b: Cu

Figure 2 shows the morphology of the Ni coatings electroplated on the Cu surface for 1, 5, 10, and 15 min, respectively. After electroplating Ni, more rough pinecone-like structures can be formed on the surface of Cu. The pinecone-like structures are mainly composed of scales with a size distribution ranging from 50–300 nm as shown in Figure 2b. As the plating time increased from 1 min to 15 min, the pinecone structures grow larger as the gap between the pinecones becomes narrow. The substrate becomes better covered after 15 min of plating.



**Figure 2.** The morphology of the Ni coating electroplated on the Ni-P/Cu surface after different plating times: a: 1 min; b: 5 min; c: 10; d: 15 min

Figure 3 compares the XRD patterns of the Mg alloy, pure Ni, Ni-P coating, and stearic acid-modified Ni-P/Cu/Ni composite coating. The Mg alloy is mainly composed of Mg and intermetallic compounds  $\text{Mg}_{17}\text{Al}_{12}$ . The Ni-P coating shows a wide peak of Ni (111), which is evidence of an amorphous structure. The amorphous structure of the Ni-P coating exhibits good corrosion resistance. After electrodeposition of Ni on Cu, it is clear that the three diffraction peaks of Ni at  $2\theta = 44.51^\circ$ ,  $52.00^\circ$  and  $76.57^\circ$  correspond to the characteristic peaks of the Ni(111), Ni(200) and Ni(220) planes of the face-centred cubic Ni crystals, respectively [24]. The other three peaks at  $2\theta$  values of  $43.64^\circ$ ,  $50.80^\circ$ , and  $74.42^\circ$  corresponding to the (111), (200), and (220) planes of copper were observed and compared with the standard powder diffraction card of JCPDS, copper file No. 04–0836[25]. The relative intensity of the Ni(200) peak in the electrodeposited Ni coating was weaker than that in pure Ni, and this result indicated that the Ni(200) crystal plane was covered by other crystal planes in the

process of electrodeposition[26], which can also explain why pinecone-like structures of the Ni coating were formed.

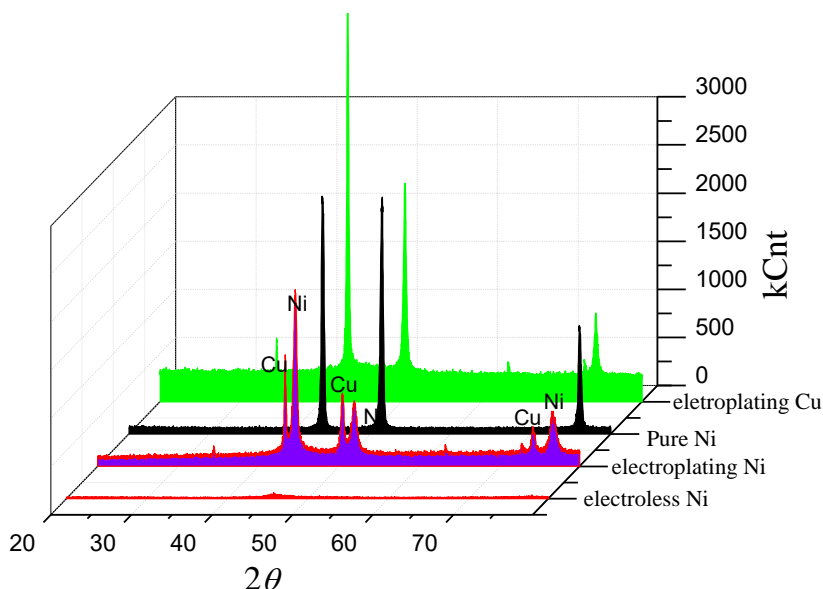


**Figure 3.** XRD patterns of the pure Ni, Ni-P coating, electroplated Cu coating and Ni-P/Cu/Ni composite coating

### 3.2 CAs of the coating

Figure 4 shows the CA change in water droplets on Ni-P/Cu/Ni and stearic acid-modified Ni-P/Cu/Ni composite coating. The Cu coating has a hydrophilic character with a CA of about 70°. As the roughness of the Ni coating increases with plating time, the contact angles will decrease with Ni plating time, and CA becomes 0° after plating Ni for 5 min. The results were consistent with Wenzel's conclusion. According to the Wenzel model[27], for a hydrophilic surface, roughness increases the surface area of the solid, which geometrically enhances hydrophilicity.

$$\cos \theta_c = r \cos \theta \quad (1)$$

where  $r$  is the roughness defined as the ratio between the real and projected solid liquid contact areas and  $\theta_c$  and  $\theta$  are the contact angles on the rough and smooth surfaces, respectively. A hierarchically micro/nano-structured Ni-P/Cu/Ni coating was prepared on the Mg alloy. Hence, the first condition was reached for the formation of a hydrophobic coating. After modifying with stearic acid, the CAs of the composite coating increase gradually from 0 to 155°. It is well-known that stearic acid contains a carboxyl group and a long alkyl chain, and Ni coating has some hydroxyl groups. In the process of modification, the reaction between a carboxyl group and a hydroxyl group takes off a molecule of water, and then the long alkyl chain is modified on the surface of the Ni coating. The second condition is then reached for the formation of a hydrophobic coating, according to the Cassie-Baxter model[28], and the hydrophobicity of the hydrophobic coating increases with the surface roughness because air is trapped in the hierarchical structure.

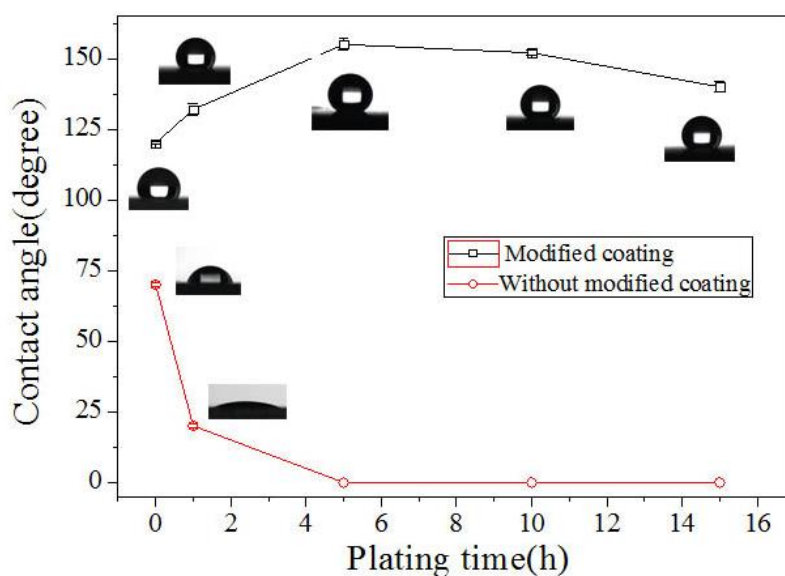


**Figure 4.** The dependence of CAs on plating time for Ni-P/Cu/Ni and stearic acid-modified Ni-P/Cu/Ni composite coating

The CA test results can be explained by Figure 5, which is a schematic of the Ni surface according to the SEM images (Figure 2). Electroplating Ni for 5 min and modifying the coating leads to superhydrophobicity because air is trapped in the hierarchical structure, which enhances the hydrophobicity. When some water or corrosive solution is dropped on the coating surface, the coating can effectively prevent the contact of the corrosive solution or water with the substrate.

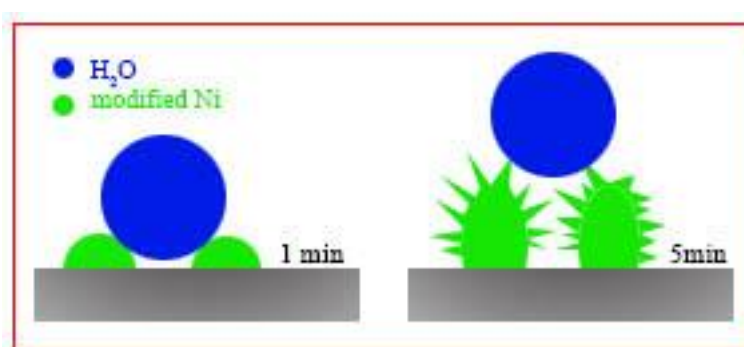


**Figure 5.** Schematic of a water droplet on the stearic acid-modified Ni-P/Cu/Ni composite coating

### 3.3 Potentiodynamic polarization characterization

The corrosion resistance of Mg alloy, Ni-P/Cu/Ni coating, and stearic acid-modified Ni-P/Cu/Ni coating was evaluated by potentiodynamic polarization, and the test results are shown in Figure 6. Electrochemical parameters related to the potentiodynamic polarization curves are listed in Table 2. A lower corrosion current density suggests a lower corrosion rate, and a positive shift in the corrosion potential represents a lower corrosion tendency. The Tafel slope is another experimental parameter that is sensitive to the structure of the surface, and a higher Tafel slope reflects a higher

resistance of the electrode reaction in the Tafel region. For the unmodified coating and modified coating, the corrosion current density  $i_{\text{corr}}$  was decreased by one or two orders of magnitude after modification. A positive shift of 1150 mV in  $E_{\text{corr}}$  was observed compared with the Mg alloy substrate. For the modified sample, the anode polarization slope ( $b_a$ ) value was higher than for the unmodified coating and Mg alloy, and an obvious passivation region was observed in the polarization curve, which suggested that a passivation film may have formed on the surface of the sample during the corrosion process[29]. The previous test results indicated that more air can be trapped on the super-hydrophobic coating surface, the air cushion was formed between coating and NaCl solution when the sample immersion in NaCl solution, that led to small contact area of surface with NaCl solution and passivation film easily formed on the modified coating surface compared with unmodified coating. Thus the modified composite coating has lower  $i_{\text{corr}}$  and higher  $E$  and  $b_a$  than the unmodified coating. The results were consistent with the conclusions of the other previous work in this area [29, 30]. It indicated that the coating exhibits a lower corrosion tendency and corrosion rate after modification by stearic acid.

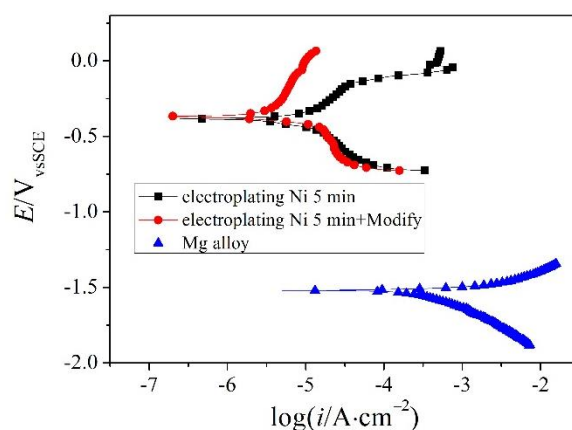


**Figure 6.** Potentiodynamic polarization curves of Mg alloy, Ni-P/Cu/Ni coating and stearic acid-modified Ni-P/Cu/Ni coating in 3.5 wt.% NaCl solution

**Table 2.** The values of the electrochemical parameters obtained from the polarization curves in Figure 6

Specimens	Mg alloy	Ni-P/Cu/Ni coating	Ni-P/Cu/Ni/stearic acid-modified coating
$E_{\text{corr}}/\text{V}_{\text{vsSCE}}$	-1.52	-0.38	-0.37
$i_{\text{corr}}/(\text{A}\cdot\text{cm}^{-2})$	$3.66\times 10^{-4}$	$1.07\times 10^{-5}$	$4.02\times 10^{-6}$
$b_a/(\text{mV}\cdot\text{dec}^{-1})$	119.34	416.32	887.61
$-b_c/(\text{mV}\cdot\text{dec}^{-1})$	156.52	431.49	785.94

### 3.4 EIS characteristics

EIS was also employed to evaluate the protective performances of the samples. The test results are shown in Figure 7. The Nyquist plots and Bode plots are presented in Figures 7(a) and (b),



respectively. Figure 7a shows that the Nyquist plot of the Mg substrate has one capacitive loop and one inductive loop. The capacitive loop is attributed to the charge transfer reaction in the electric double layer formed at the interface between the sample surface and the corrosive medium[31], and the inductive loop is attributed to the pit corrosion on the Mg alloy surface[1]. The results indicated the poor corrosion resistance of Mg alloy in NaCl solution and that the pitting corrosion has already begun to form on the surface. The unmodified film and modified film have one capacitive loop. The EIS parameters of the Mg alloy, Ni-P/Cu/Ni coating and Ni-P/Cu/Ni/stearic acid-modified coating are listed in Table 3. The resistance of the charge transfer ( $R_{ct}$ ) between the modified film surface and the corrosive medium ( $4.3 \times 10^4 \Omega \cdot \text{cm}^2$ ) was bigger than that unmodified sample ( $7670 \Omega \cdot \text{cm}^2$ ) and Mg alloy substrate ( $128.1 \Omega \cdot \text{cm}^2$ ), the value of  $R_{ct}$  of modified coating was nearly two times than other related report ( $R_{ct}=17652 \Omega \cdot \text{cm}^2$ )[13]. The constant phase element (CPE) behaviour is generally attributed to the distributed surface reactivity, surface inhomogeneity, roughness or electrode porosity[32]. The CPE was defined by two values,  $Y_0$  and  $n$ . Modified film and unmodified sample have the similar  $n$  value, but the  $CPE-Y_0$  value of modified film ( $9.12 \times 10^{-5} \text{ S} \cdot \text{sec}^n \cdot \text{cm}^{-2}$ ) was lower than unmodified sample ( $6.2 \times 10^{-4} \text{ S} \cdot \text{sec}^n \cdot \text{cm}^{-2}$ ), indicated that modified film with better capacitance characteristics which can effectively isolate the substrate from the corrosive solution[33]. The EIS results consistent with the polarization results, which indicated that the modified film could effectively enhance the corrosion resistance of Mg alloy compared with the unmodified film and Mg substrate.

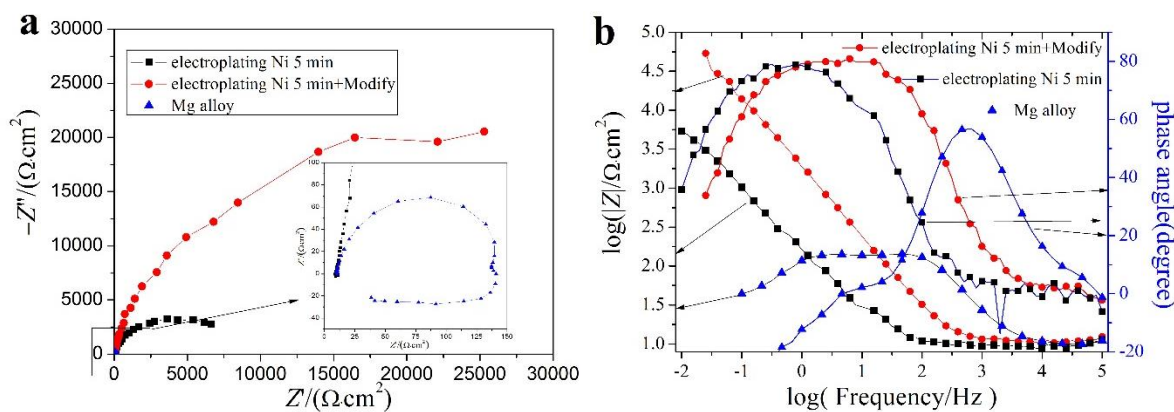


**Figure 7.** EISs of Mg alloy, Ni-P/Cu/Ni coating and stearic acid-modified Ni-P/Cu/Ni coating in 3.5wt.% NaCl solution: a: Nyquist plots; b: Bode plots

**Table 3.** The values of the electrochemical parameters obtained from the EISs in Figure 7.  $R_s$ , resistance of solution;  $R_{ct}$ , charge transfer resistance;  $CPE-Y_0$ , constant phase element- $Y_0$

Specimens	Mg alloy	Ni-P/Cu/Ni coating	Ni-P/Cu/Ni/stearic acid-modified coating
$R_s/(\Omega \cdot \text{cm}^2)$	10.37	9.65	10.95
$R_c/(\Omega \cdot \text{cm}^2)$	128.1	7670	$4.3 \times 10^4$
$CPE-Y_0/(\text{S} \cdot \text{sec}^n \cdot \text{cm}^{-2})$	$8.27 \times 10^{-6}$	$6.2 \times 10^{-4}$	$9.12 \times 10^{-5}$
$CPE-n$	0.95	0.91	0.92

#### 4. CONCLUSIONS

A super-hydrophobic composite coating was prepared on AZ31B via electroless Ni-P coating, electroplating Cu, electroplating Ni and modification with stearic acid. The micro/nanometre-scale binary rough structures surface was formed via electroless Ni-P coating for 90 min, electroplating Cu for 15 min, and electroplating Ni for 5 min. The CA of the coating was about 155° after the prepared coating was modified in 1% stearic acid ethanol solution for 2 h. The corrosion resistance of the super-hydrophobic composite coating was characterized by potentiodynamic polarization and EIS. The potentiodynamic polarization results showed that the super-hydrophobic composite coating had lower  $i_{\text{corr}}$  ( $4.02 \times 10^{-6} \text{ A} \cdot \text{cm}^{-2}$ ) and higher  $E$  ( $-0.37 \text{ V}_{\text{vsSCE}}$ ) than the unmodified coating. The EIS results showed that the resistance of the charge transfer between the modified film surface and the corrosive medium was bigger than that between the unmodified film surface and the corrosive medium. All of the test results indicated that the modified composite coating exhibited higher corrosion resistance than the unmodified coating.

#### ACKNOWLEDGEMENT

This study are jointly funded by the National Natural Science Foundation of China (51501157, 51604180), the Fundamental Research Funds of China West Normal University (17B005), and the Chemical Synthesis and Pollution Control Key Laboratory of Sichuan Province (CSPC2014-4-2).

#### References

1. Z. Song, Z. Xie, G. Yu, B. Hu, X. He, and X. Zhang, *J. Alloys Compd.*, 623(2015) 274-281.
2. T. Xiang, S. Ding, C. Li, S. Zheng, W. Hu, J. Wang, and P. Liu, *Mater. Des.*, 114(2017) 65-72.
3. N.V. Phuong, M. Gupta, and S. Moon, *Prog. Org. Coat.*, 102, Part B(2017) 144-150.
4. A.D. Forero López, I.L. Lehr, and S.B. Saidman, *J. Alloys Compd.*, 702(2017) 338-345.
5. L.-Y. Cui, S.-D. Gao, P.-P. Li, R.-C. Zeng, F. Zhang, S.-Q. Li, and E.-H. Han, *Corros. Sci.*, 118(2017) 84-95.
6. Y. Zhang, S. Tang, J. Hu, and T. Lin, *Corros. Sci.*, 111(2016) 334-343.
7. J. Zhang, C. Gu, Y. Tong, W. Yan, and J. Tu, *Adv. Mater. Interfaces*, 3(2016) 1500694.
8. J.A. Fairfield, C.G. Rocha, C. O'Callaghan, M.S. Ferreira, and J.J. Boland, *Nanoscale*, 8(2016) 18516-18523.
9. F. Zhang, L. Zhao, H. Chen, S. Xu, D.G. Evans, and X. Duan, *Angew. Chem. Int. Ed. Engl.*, 47(2008) 2466-9.
10. C. Gu, J. Lian, J. He, Z. Jiang, and Q. Jiang, *Surf. Coat. Technol.*, 200(2006) 5413-5418.
11. D. Zang, R. Zhu, W. Zhang, X. Yu, L. Lin, X. Guo, M. Liu, and L. Jiang, *Adv. Funct. Mater.*, 27(2017) 1605446.
12. Q. Liu, D. Chen, and Z. Kang, *ACS Appl. Mater. Interfaces*, 7(2015) 1859-67.
13. Y. Liu, X. Yin, J. Zhang, S. Yu, Z. Han, and L. Ren, *Electrochim. Acta*, 125(2014) 395-403.
14. Z. Wang, Q. Li, Z. She, F. Chen, and L. Li, *J. Mater. Chem.*, 22(2012) 4097.
15. F. Tian, A. Hu, M. Li, and D. Mao, *Appl. Surf. Sci.*, 258(2012) 3643-3646.
16. H. Ogihara, T. Katayama, and T. Saji, *J. Mater. Chem.*, 21(2011) 14890.
17. R. Gan, D. Wang, Z.H. Xie, and L. He, *Corros. Sci.*, 123 (2017) 147-157.
18. Z.P. Zhang, Y.H. Qi, Y. Zhang, G.K. Mo, and J.Z. Wang, *Mater. Sci. Forum*, (2010) 1900-1903.
19. J.L. Song, W.J. Xu, Y. Lu, X. Liu, and J. Sun, *Mater. Corros.*, 64(2013) 979-987.
20. J. Zhao, X. Xie, and C. Zhang, *Corros. Sci.*, 114(2017) 146-155.

21. D. Li, F. Chen, Z.H. Xie, S. Shan, and C.J. Zhong, *J. Alloys Compd.*, 705(2017) 70-78.
22. Z.H. Xie, F. Chen, S.R. Xiang, J.L. Zhou, Z.W. Song, and G. Yu, *J. Electrochem. Soc.*, 162(2015) D115-D123.
23. D. Yan, G. Yu, B. Hu, J. Zhang, Z. Song, and X. Zhang, *J. Alloys Compd.*, 653(2015) 271-278.
24. Z. She, Q. Li, Z. Wang, L. Li, F. Chen, and J. Zhou, *Chem. Eng. J.*, 228(2013) 415-424.
25. T. Theivasanthi and M. Alagar, *Epl*, 53(2010) 169-175.
26. Z. Chen, F. Tian, A. Hu, and M. Li, *Surf. Coat. Technol.*, 231(2013) 88-92.
27. R.N. Wenzel, *Ind.eng.chem*, 28(1936) 988-994.
28. A.B.D. Cassie, *Discuss. Faraday Soc.*, 3(1948) 11-16.
29. Y. Wang, Z. Gu, Y. Xin, N. Yuan, and J. Ding, *Colloids Surf. Physicochem. Eng. Aspects*, 538(2018) 500-505.
30. Y. Zhong, J. Hu, Y. Zhang, and S. Tang, *Appl. Surf. Sci.*, 427(2018) 1193-1201.
31. H. Zhao, S. Cai, Z. Ding, M. Zhang, Y. Li, and G. Xu, *Rsc Adv.*, 5(2015) 24586-24590.
32. Y. Song, D. Shan, R. Chen, and E.-H. Han, *Corros. Sci.*, 51(2009) 1087-1094.
33. Z. Song, G. Yu, Z. Xie, B. Hu, X. He, and X. Zhang, *Surf. Coat. Technol.*, 242(2014) 83-91

© 2018 The Authors. Published by ESG ([www.electrochemsci.org](http://www.electrochemsci.org)). This article is an open access article distributed under the terms and conditions of the Creative Commons Attribution license (<http://creativecommons.org/licenses/by/4.0/>).